NANO LETTERS

pubs.acs.org/NanoLett
Letter

Development of Chemical Tags for Universal Lipid Nanoparticle Visualization and Tracking in 2D and 3D Imaging

Hannia V. Balcorta, Mario Y. Mata Corral, Angel Gallegos, Jael Chavez, Jose Perez, Sivasai Balivada, Sylvia L. Natividad-Diaz, and Wilson Poon*

Cite This: *Nano Lett.* 2025, 25, 7682–7689
Read Online

ABSTRACT: Precise delivery of therapeutic agents to specific cells and subcellular compartments is crucial for effective disease treatment. Lipid nanoparticles (LNPs) are promising drugs and gene nanocarriers, but understanding their transport within cells and tissues remains limited. We developed SPARKLE (Strategic Peptide, Anchored, Retained, and Kept after Lipid Elimination), a fluorescent peptide tag designed to track LNPs with advanced optical imaging techniques that involve lipid disruption (e.g., cell permeabilization or tissue clearing). Unlike conventional lipophilic dyes that wash out during lipid disruption, SPARKLE tags are retained and fluorescently mark the positions of LNPs. As proof of concept, we demonstrated the utility of SPARKLE tags by tracking LNPs *in vitro* using the cell painting assay and *in vivo* within tissues using CLARITY tissue clearing and 3D light-sheet microscopy. SPARKLE tags can offer valuable insights into LNP behavior in biological environments, enhancing the understanding of their targeting and cargo release for clinical translation.

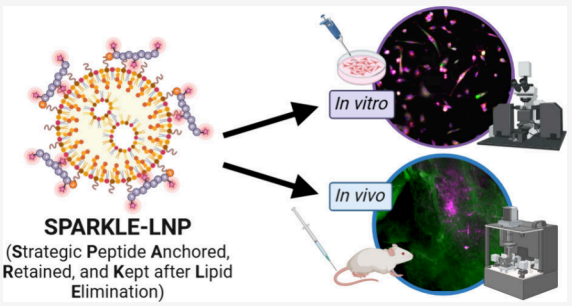

KEYWORDS: *nanomedicine, lipid nanoparticles, bioconjugate chemistry, cell painting, fluorescence imaging*

The delivery of medical agents to a specific diseased tissue or cell is critical for diagnosing and treating patients.[1] Nanomedicine is a promising platform for medical applications because nanoparticles can be used to improve the delivery of a wide variety of chemotherapeutics,[2] contrast agents,[3] immunotherapies,[4] and gene therapies[5] in patients. By precisely engineering nanoparticles with specific size, shape, and chemistries, we can create nanomedicines that enhance the solubility of hydrophobic drugs,[6] extend blood circulation time,[7] control temporal release of drugs,[8] and alter biodistribution.[9] Lipid nanoparticles (LNPs) are emerging as the most promising class of nanomedicines for clinical applications.[10] Most notably are the lipid nanoparticle-based vaccines that were vital in protecting the populace during the SARS-2 pandemic.[11,12] Research in developing the next generation of lipid nanoparticles that can carry larger drug or gene payloads, are less likely to trigger adverse immune reactions upon administration, and can more specifically target exact cell types in the body are ongoing.[13] Despite advances in nanomaterials engineering, the optimal design for nanoparticles to reach a specific biological target in the body after administration is unclear.[14] There is limited understanding of how nanoparticle physical and chemical properties affect how they interact with their biological environments in the body to reach the desired target and release their cargo. Understanding how nanoparticles interact at the organ, suborgan, cellular, and subcellular levels will improve the design of more efficient drug carriers for precise delivery of therapeutic agents and genes to target sites in patients for any disease.[15]

There are currently limited methods to study the interaction of lipid nanoparticles with cells and tissues. Radioisotopes can be used to label lipids in the nanoparticle and imaged using positron emission tomography (PET) or quantified using scintillation counting.[16] However, positron emission tomography is mostly used for whole body imaging to visualize organ-level distribution and lacks the resolution necessary for cellular or subcellular localization of nanoparticles.[17] The use of radioactive atoms also creates disposal problems, requires trained personnel, and presents logistical challenges for shelf life of the radiotracers in the experimental workflow.[18] Fluorescent labeling is also used to study lipid nanoparticle behavior in cells and tissues. Fluorescent labels can be multiplexed for imaging by using dyes with different fluorescence spectra for lipids and cargoes. However, conventional fluorescence imaging has limited depth due to the scattering of light through lipid interfaces from cell membranes in whole opaque tissues. Subcellular resolution with

Received: January 14, 2025
Revised: April 8, 2025
Accepted: April 9, 2025
Published: May 4, 2025

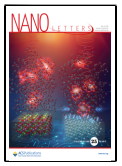

https://doi.org/10.1021/acs.nanolett.5c00311
Nano Lett. 2025, 25, 7682–7689

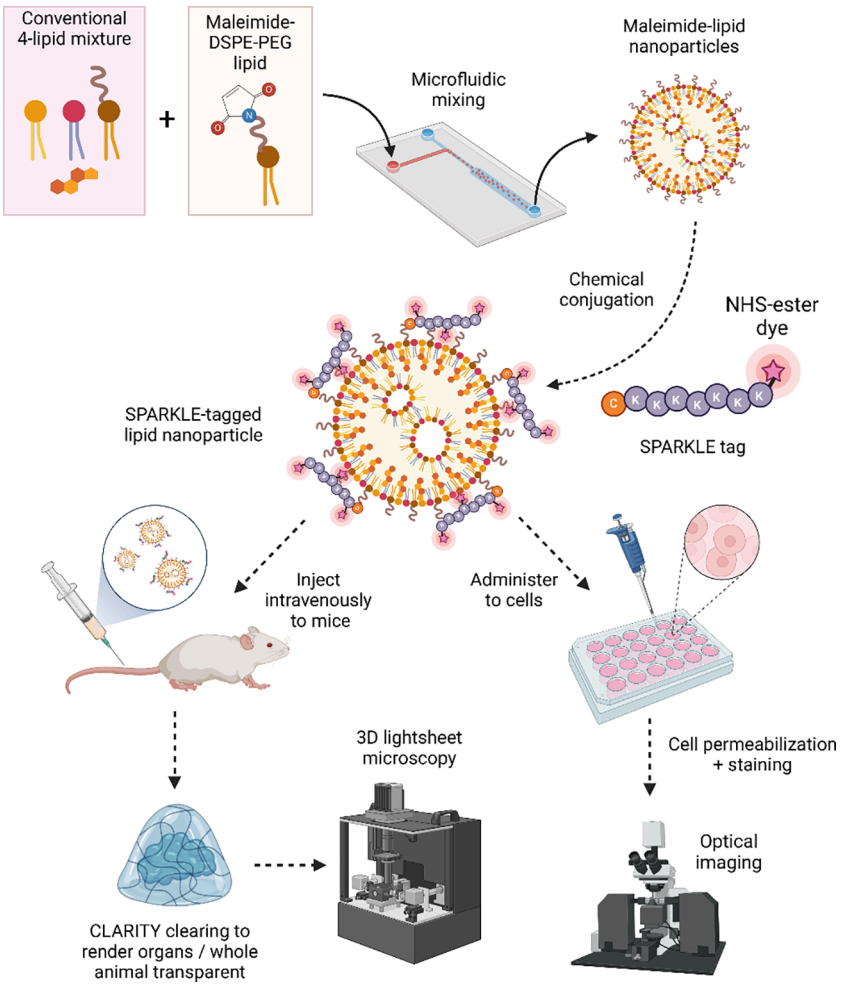

Figure 1. Design and scheme for the synthesis and testing of SPARKLE tags as chemically labeled, cross-linkable, fluorescent tags for lipid nanoparticles. Figure created with Biorender.com.

fluorescence is also difficult unless complex optical setups for super-resolution imaging are made available. Quantification of fluorescence is also semiquantitative and prevents direct comparison between different nanoparticle designs and experiments due to environmental effects on the optical properties of fluorescent dyes and the possibility of the fluorescent dyes to dissociation from the nanoparticle in biological environments.[19]

Fluorescent lipophilic dyes, such as DiI (1,1′-dioctadecyl-3,3,3′3′-tetramethylindocarbocyanine perchlorate) and DiO (3,3′-dioctadecyloxacarbocyanine perchlorate), are used conventionally to label LNPs.[20] These lipophilic dye molecules have long hydrophobic tails that allow them to become embedded throughout the interior of LNPs and track their movement, distribution, and cellular uptake by using fluorescence-based imaging techniques. Sample preparation for many fluorescence-based imaging techniques requires the addition of chemical reagents that disintegrate or remove lipid nanoparticles in cells and tissues. For example, immunofluorescence may involve the addition of detergent to permeabilize cellular membranes for intracellular staining;[21] histology uses xylene as a clearing agent for wax infiltration that can remove lipids and fat;[22,23] and tissue clearing-enabled imaging such as CLARITY and expansion microscopy use detergents to remove cellular lipid membranes to reduce optical scattering interfaces.[24] As such, these lipophilic dyes and lipid nanoparticles will become disassociated and disintegrated during the sample preparation process and are therefore incompatible with these imaging techniques. Other functional tracking methods, which involve using transgenic animal models to quantitate lipid nanoparticle delivery through fluorescent or luminescent reporter protein expression, can lead to misrepresentation in the spatial distribution and temporal kinetics of their delivery.[25]

To address these issues, we developed a new chemical tag for lipid nanoparticles called SPARKLE (Strategic Peptide Anchored, Retained, and Kept after Lipid Elimination) that can be retained during sample preparation for 2D and 3D microscopy and fluorescently mark the positions of LNPs *in vitro*. For our SPARKLE tag design and approach, we used the conventional SM-102-based four-lipid component recipe (Moderna SPIKEVAX formulation) and added DSPE-PEG(2000)-maleimide as a fifth lipid component. This enables conjugation of the SPARKLE peptide tag to the lipid nanoparticles. The maleimide functional group of DSPE-PEG(2000)-maleimide reacts with the sulfhydryl group in the terminal cysteine (C) amino acid residue of the SPARKLE peptide tags to link the peptide to the lipid nanoparticle. The multiple lysine (K) amino acid residues in the SPARKLE peptide tag contain primary amino groups in the side chain that can be used to conjugate fluorescent dye, such as Alexa Fluor 647 (AF647), to the lipid nanoparticle via NHS-ester

https://doi.org/10.1021/acs.nanolett.5c00311
Nano Lett. 2025, 25, 7682−7689

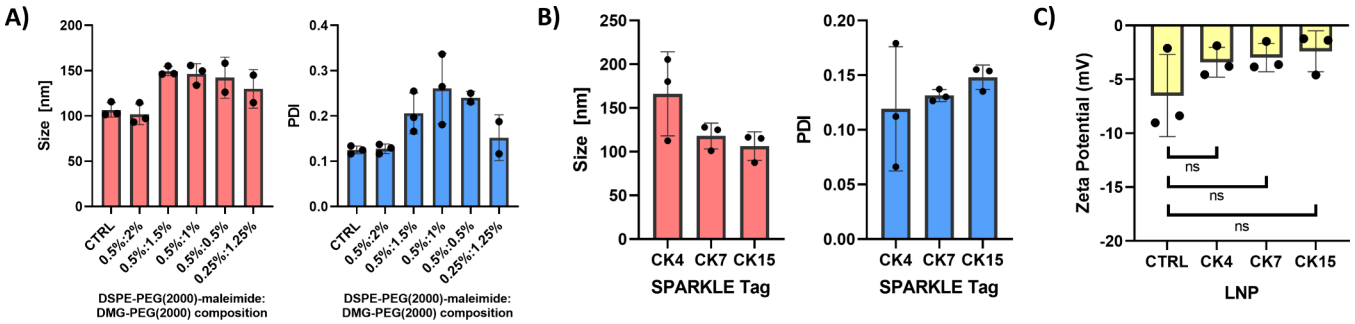

Figure 2. LNP characterization by dynamic and electrophoretic light scattering for (A) size and polydispersity of varying DSPE-PEG-maleimide:DMG-PEG formulations; (B) size and polydispersity of varying SPARKLE tags; and (C) zeta potential (surface charge) measurement for SPARKLE tag formulations. Data are displayed as mean ± standard deviation with a sample size of $n = 3$. CTRL indicates the control lipid nanoparticles.

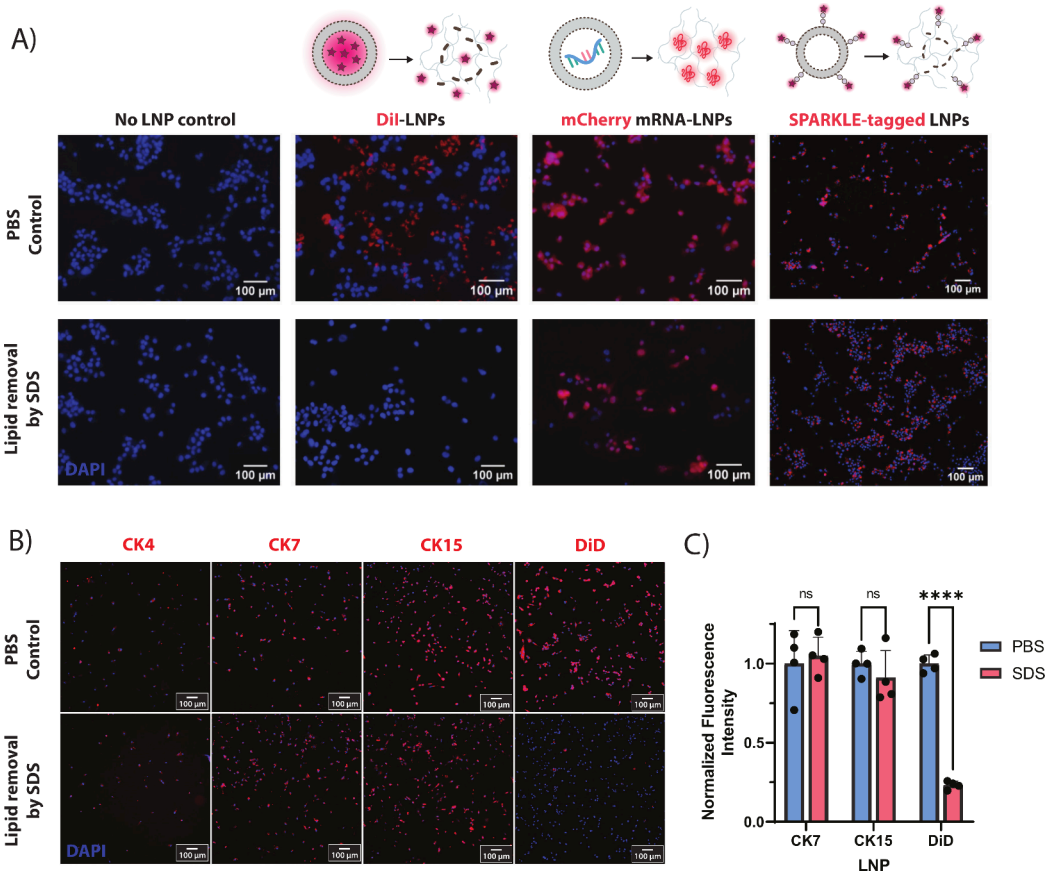

Figure 3. (A) Representative fluorescence images of various LNPs in U87-MG cells before and after lipid removal with SDS. Blue represents nuclei counterstaining. Red represents DiI lipophilic dye, mCherry mRNA-expression, or AF647-SPARKLE CK7 tag as indicated. (B) Representative fluorescence images of retention of LNP with various SPARKLE tags and encapsulated DiD lipophilic dye (1,1′-dioctadecyl-3,3,3′,3′-tetramethylindodicarbocyanine, 4-chlorobenzenesulfonate salt) in U87-MG cells before and after lipid removal. (C) Quantification of fluorescence intensity retention after lipid removal of LNPs with various SPARKLE tags and encapsulated DiD lipophilic dye. Scale bars represent 100 μm. Data are displayed as mean ± standard deviation with a sample size of $n = 4$. Statistical analysis performed by unpaired test with Holm−Sidak multiple comparisons method ($\alpha = 0.05$), where ns = not significant and **** = $p < 0.0001$.

chemistry (see Figure S1). The remaining unreacted lysine amino acid residues can then be used to cross-link the lipid nanoparticles into the cell during fixation and be retained even after lipid removal during membrane permeabilization and staining (Figure 1).

First, we experimented with the addition of DSPE-PEG(2000)-maleimide to the conventional lipid mixture in varying percentages to determine how it affects the LNP size and polydispersity as a proxy for colloidal stability. We tested five different ratios of DSPE-PEG(2000)-maleimide:DMG-PEG(2000), specifically 0.5 mol %:2 mol %, 0.5 mol %:1.5 mol %, 0.5 mol %:1 mol %, 0.5 mol %:0.5 mol %, and 0.25 mol %:1.25 mol %. After characterizing the LNP formulations using dynamic light scattering to determine their size and polydispersity, we chose the ratio containing 0.5% DSPE-PEG(2000)-maleimide and 2% DMG-PEG(2000), as it possessed similar physicochemical properties to the control LNP with no DSPE-PEG(2000)-maleimide, with a mean z-

https://doi.org/10.1021/acs.nanolett.5c00311
Nano Lett. 2025, 25, 7682−7689

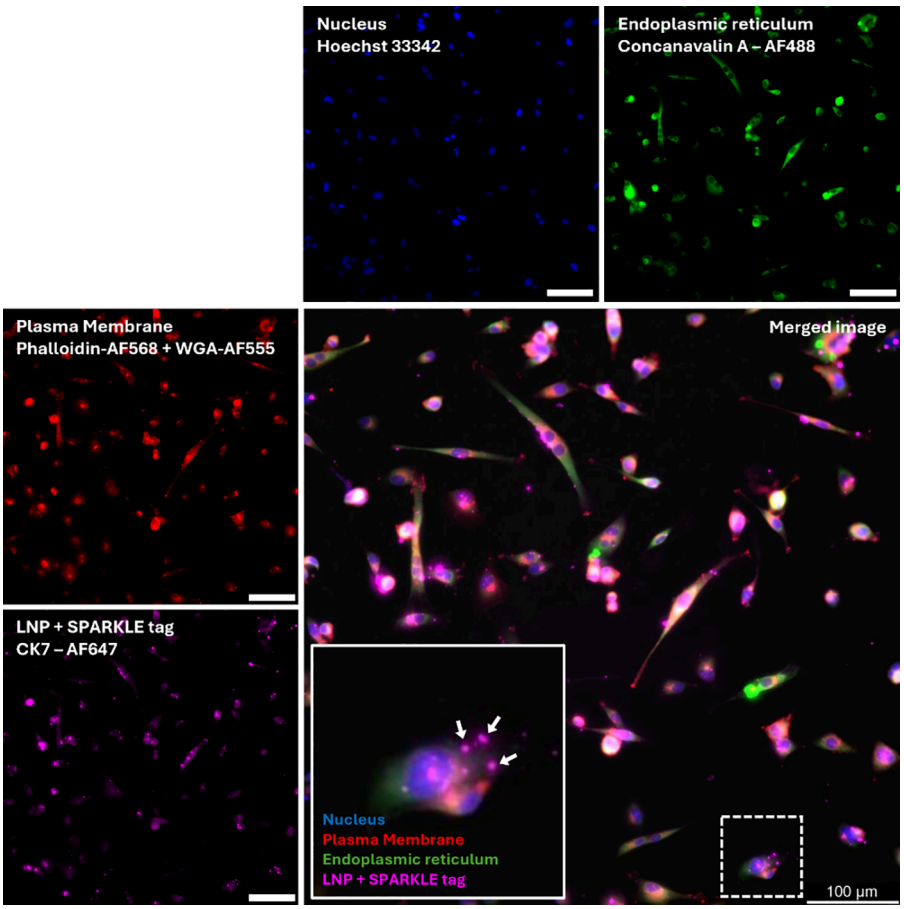

Figure 4. Representative cell painting images demonstrating retained SPARKLE tags within U87-MG cells after membrane permeabilization and staining along with labeled organelles and subcellular regions. Nuclei are stained blue with Hoechst 33342, endoplasmic reticulum and golgi apparati are stained green with concanavalin A-AF488, the plasma membrane is stained with phalloidin-AF568 and wheat germ agglutinin (WGA)-AF555, and CK7-SPARKLE-LNPs are labeled with AF647. White arrows indicate SPARKLE-LNP puncta inside cells. Scale bars represent 100 μm.

average size of 114.8 nm and polydispersity index of 0.12 (Figure 2A). The final lipid composition molar ratio of this optimized LNP was 50 mol % SM-102, 10 mol % 1,2-DSPC, 37.5 mol % cholesterol, 2 mol % DMG-PEG(2000), and 0.5 mol % DSPE-PEG(2000)-maleimide. Following this, we optimized the SPARKLE tag length by conjugating three different peptide sequences that varied in the number of lysine (K) residues: CK4, CK7, and CK15, and AF647 dye to form SPARKLE-LNPs to determine which design would provide simultaneously sufficient fluorescence signal and cross-linking into the surrounding tissue for retention (Figures 2B and S2). Additionally, we measured the change in surface charge (zeta potential) of the SPARKLE-LNPs due to the increase in number of positive charges from the lysine groups present in the peptides as compared to the unconjugated DSPE-PEG(2000)-maleimide control LNPs, which yielded non-statistically significant results (Figure 2C). Furthermore, we measured the impact of the SPARKLE-tag conjugation on the apparent pK_a of LNPs using the TNS method.[26] The apparent pK_a of a LNP is the result of the average ratio of all the ionized to deionized groups in the LNP and is used as a metric for evaluating potential endosomal escape behavior of the LNP cargo as well as the stability, potency, and toxicity of LNPs. As shown in Figure S3, the apparent pK_a values for maleimide-LNPs, CK7-LNPs (peptide tag only with no dye), and AF647-CK7-LNPs are 6.98, 6.93, and 6.55, respectively. Although there is slight modification of the apparent pK_a due to the presence of SPARKLE-tags, these LNPs still exhibit apparent pK_a values within the optimum values of 6 to 7 as described in literature and used in the clinic.[26]

To test the cross-linking ability and delipidation survival of the SPARKLE-tagged lipid nanoparticles, we administered the SPARKLE-LNPs to U87-MG cells, a human glioblastoma cell line (Figure 3). To compare our SPARKLE-LNPs with existing lipid nanoparticle tracking methods, we also separately administered LNPs encapsulating DiI lipophilic dye and LNPs encapsulating mCherry reporter mRNA (Figures S4 and S5) as controls since these LNPs should not cross-link within cells after lipid removal.[27] U87-MG cells were treated with LNPs for 24 h, then fixed with paraformaldehyde, incubated with SDS delipidation solution for 4 h, and washed before fluorescence microscopy imaging. As shown in Figure 3, DiI-LNPs did not survive lipid removal, as there was no retention of the DiI fluorescence signal. For mCherry mRNA-LNPs, mCherry reporter protein expression was retained after lipid removal, but this was from the cross-linked mCherry protein and not the LNP itself. For AF647-SPARKLE-CK7 LNPs, the fluorescence signal was retained after lipid removal and demonstrates the cross-linking ability and delipidation survival of the SPARKLE tag. We also confirmed that the SPARKLE-tagged LNPs were not toxic to U87-MG cells using the XTT assay (Figure S6). This led us to further experiments to quantify the fluorescence signal retention.

https://doi.org/10.1021/acs.nanolett.5c00311
Nano Lett. 2025, 25, 7682−7689

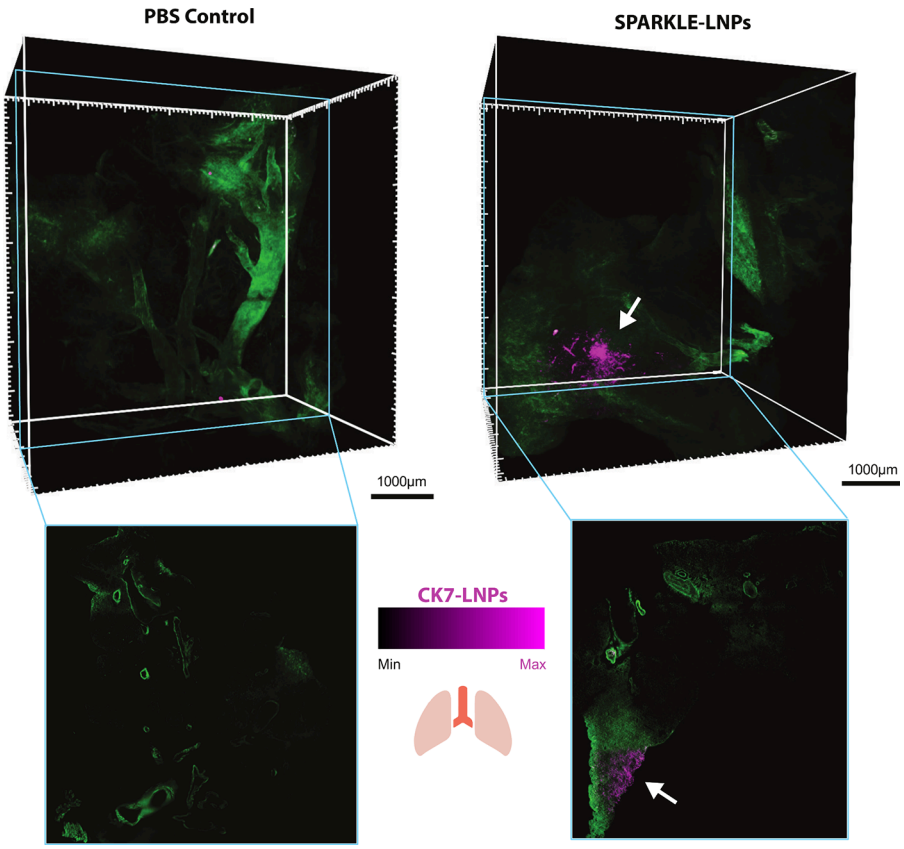

Figure 5. Representative 3D light-sheet imaging of CLARITY-treated mouse lung tissues 1 h post administration with PBS or AF647-CK7-SPARKLE-LNPs. Both three-dimensional volumes and corresponding two-dimensional insets of lung tissue are shown. Green represents tissue autofluorescence for anatomical landmarking, and pink indicates AF647-CK7-SPARKLE-LNPs. White arrows indicate high concentration of LNP accumulation.

We administered SPARKLE-LNPs with CK4, CK7, and CK15 (all labeled with AF647) and control LNPs encapsulating DiD lipophilic dye (Figure S4) into U87-MG cells and performed fixation, delipidation, and fluorescence imaging studies as before (Figures 3B and S7). We quantified the retention of fluorescence in images before and after delipidation using FIJI to assess the effect of the number of lysine residues on the effectiveness of our SPARKLE tags (Figure 3C). We found that CK7 and CK15 SPARKLE tags demonstrated high retention, with 104.8 ± 11.9% and 91.0 ± 17.3% of their fluorescence intensity retained after delipidation, respectively. On the other hand and as expected, DiD-LNPs did not have sufficient retention, demonstrating only 23.2 ± 2.6% retention after delipidation. Interestingly, CK4 SPARKLE tags were only weakly fluorescent before or after delipidation, which hindered imaging and was excluded from our image analysis. Since CK4 has fewer lysine residues compared to CK7 and CK15, its cross-linking efficiency and capacity are lower, leading to reduced retention. The greater the number of lysine residues available for cross-linking, the more likely the peptide tag will be retained and the LNP position can be marked. We believe that 4 lysine residues are not enough to simultaneously be conjugated with AF647 dye and cross-link into cells to be tracked, whereas 7 and 15 lysine residues performed well for LNP tracking.

To demonstrate the utility of our now optimized CK7-SPARKLE-LNPs, we performed a cell painting assay. The cell painting assay captures diverse cellular phenotypes through high-content imaging of multicolor fluorescently labeled organelles and subcellular compartments[28,29] and can be useful in identifying novel nanoparticle cell tropism, entry and trafficking mechanisms, and cellular response to nanomedicines. Due to the staining of intracellular compartments, the cell painting assay involves a detergent step which would make it incompatible with conventionally labeled LNPs (Figure S8). We modified the cell painting assay by replacing the mitochondria channel (originally using MitoTracker Deep Red FM) with AF647-labeled CK7-SPARKLE-LNPs to track LNP uptake and subcellular localization. We show in Figure 4 that SPARKLE-LNPs can be successfully retained and visualized in relation to other cellular organelles with the cell painting assay. Specifically, we were able to identify AF647-labeled puncta inside U87-MG cells that are most likely endolysosomes following SPARKLE-LNP uptake by cells 16 h post administration (Figure S9). This visual representation provides a clear demonstration of the effectiveness of the SPARKLE-LNPs for subcellular tracking and potential use in high-throughput, high-content imaging-based nanoparticle screens.

We next tested the compatibility of SPARKLE-LNPs *in vivo* with CLARITY tissue clearing and light-sheet imaging. CLARITY is a tissue-clearing technique that uses a hydrogel method to eliminate lipids from the biological system while preserving the integrity of proteins and other tissue structures.[30] This technique consists of infusing a hydrogel into the tissue, where it proceeds to cross-link with most biological molecules, except for lipids. Next, SDS buffer is used to encapsulate the uncross-linked lipids into micelles,

https://doi.org/10.1021/acs.nanolett.5c00311
Nano Lett. 2025, 25, 7682−7689

facilitating their removal from biological samples.[31] This approach plays a crucial role in safeguarding essential anatomical structures for microscopy-based examinations of central nervous systems, proteins, and nucleic acids.[31] We intravenously administered AF647-CK7-SPARKLE-LNPs or PBS (as control) into BALB/cJ mice and collected the lungs 1 h postadministration. The lungs were fixed, washed, and cleared using passive CLARITY tissue clearing.[32] 3D tissue imaging with PBS or AF647-CK7-SPARKLE LNPs was performed using light-sheet microscopy (Figure 5). We show that SPARKLE-LNPs can be retained and visualized in lung and other tissues for suborgan level biodistribution with some selective regional preferences (Video S1 and Figure S10). We anticipate that using the SPARKLE-tag approach can be useful in studying the *in vivo* behavior of LNPs due to its compatibility with tissue clearing and 3D imaging to enable greater depth and increased volumetric visualization of nanoparticle biodistribution in intact whole tissues.

Due to the limited tools available to look at the interaction of lipid nanoparticles with cells and tissues, most current lipid nanoparticle research focuses on organ level biodistribution studies or quantifying downstream functional readouts from the delivered cargo. As such, the cellular and subcellular delivery process of lipid nanoparticles remains understudied. Previously, peptide tags have been developed to label liposomes for visualization following tissue clearing.[33] REMNANT, as reported by Syed et al., also uses primary amines in lysine residues of the peptide tag to cross-link nanoparticles into tissues and was demonstrated to be compatible with liposomes and PLGA nanoparticles. REMNANT simultaneously uses both thiol-maleimide and DBCO-azide click chemistry conjugation to attach their peptide tag to nanoparticles. Recently, Zaleski et al. have shown that DBCO conjugation chemistry can have an impact on the toxicity and biodistribution of lipid nanoparticles as mediated by complement activation.[34] In contrast, SPARKLE, as reported here, uses only thiol-maleimide functionalization, which simplifies the conjugation scheme and removes the possibility of DBCO-azide-mediated immunogenicity. In addition, we investigated and optimized the SPARKLE tag concentration and tag length to minimize changes to both the LNP physiochemical properties and cell phenotype. The development of our new chemical tags greatly increases the availability of LNP tracking approaches *in vitro* and *in vivo* due to enabling LNP survival during delipidation steps. By providing a means to visualize and quantify lipid nanoparticles at subcellular resolution and in whole intact tissues, we can gain mechanistic insight into the delivery process of how lipid nanoparticles deliver their cargo to cells. This will also permit the rigorous testing of how different chemical compositions and surface chemistries of lipid nanoparticles change how they get taken up by cells or processed by the body. In turn, it will be possible to rationally test and develop better lipid nanoparticle designs that have higher payload capacity, less immunogenicity and off-target adverse side effects, and more efficiency at reaching specific cellular and subcellular biological targets in the body. The broader impact of this work is that these tools can be adapted to study other lipid-based biological processes such as exosome production and transport between cells for intercellular communication, and enveloped virus or virus-like particle (VLP) membrane fusion with cells during infection. Overall, we envision that SPARKLE tags can be applied to the research and development of any lipid-based pharmaceuticals for the benefit of more patients.

In summary, we report the development of chemical peptide tags, termed SPARKLE (Strategic Peptide Anchored, Retained, and Kept after Lipid Elimination), that enable LNP retention during delipidation steps for *in vitro* and *in vivo* tracking studies. We first optimized the mol % and length of SPARKLE tag necessary for retention by showing that LNPs with 0.5 mol % DSPE-PEG(2000)-maleimide and SPARKLE tags containing 7 or 15 lysines were retained at close to 100% in cells after delipidation with SDS. Next, we demonstrated the tracking of SPARKLE-tagged LNPs to subcellular resolution using the cell painting assay in U87-MG cancer cells, whereas conventional lipophilic dye loaded LNPs were not able to be visualized in comparison. Finally, we showed that the *in vivo* biodistribution of SPARKLE-tagged LNPs could be mapped in mouse lung tissues and visualized by 3D light-sheet imaging following weeks of delipidation by CLARITY tissue clearing. We anticipate that our SPARKLE tags approach can be used to provide insights into how LNPs interact with cells and tissues, enabling the design of more targeted LNP therapeutics for optimized drug and gene delivery to benefit patients.

■ ASSOCIATED CONTENT

Supporting Information

The Supporting Information is available free of charge at https://pubs.acs.org/doi/10.1021/acs.nanolett.5c00311.

Video S1, 3D rendering of mouse lung after tissue clearing with SPARKLE-LNPs (MP4)

Methods and materials; scheme for SPARKLE tag chemistry, dye conjugation, cross-linking, and retention; MS and HPLC characterization data for custom peptides; UV−visible spectroscopy of LNPs with different SPARKLE tags conjugated with AF647; measurement of apparent pK_a values of various LNPs; characterization data for mCherry-mRNA LNPs; cell viability data of SPARKLE-LNPs; fluorescence images of U87-MG cells administered with different SPARKLE-LNPs with cell painting assay; fluorescence images showing colocalization of SPARKLE-LNPs with endo-lysosomes; and 3D rendered images of mouse livers containing SPARKLE-LNPs (PDF)

■ AUTHOR INFORMATION

Corresponding Author

Wilson Poon − *Department of Metallurgical, Materials, and Biomedical Engineering, College of Engineering and Border Biomedical Research Center, The University of Texas at El Paso, El Paso, Texas 79968, United States;* orcid.org/0000-0003-2192-3077; Email: wpoon@utep.edu

Authors

Hannia V. Balcorta − *Department of Metallurgical, Materials, and Biomedical Engineering, College of Engineering, The University of Texas at El Paso, El Paso, Texas 79968, United States*

Mario Y. Mata Corral − *Department of Metallurgical, Materials, and Biomedical Engineering, College of Engineering, The University of Texas at El Paso, El Paso, Texas 79968, United States*

Angel Gallegos − *Department of Metallurgical, Materials, and Biomedical Engineering, College of Engineering, The*

https://doi.org/10.1021/acs.nanolett.5c00311
Nano Lett. 2025, 25, 7682−7689

University of Texas at El Paso, El Paso, Texas 79968, United States

Jael Chavez − *Department of Metallurgical, Materials, and Biomedical Engineering, College of Engineering, The University of Texas at El Paso, El Paso, Texas 79968, United States*

Jose Perez − *Department of Metallurgical, Materials, and Biomedical Engineering, College of Engineering, The University of Texas at El Paso, El Paso, Texas 79968, United States; 3D Microphysiological Systems Laboratory (3DMPSL), The University of Texas at El Paso, El Paso, Texas 79968, United States*

Sivasai Balivada − *Department of Biological Sciences, College of Science and Border Biomedical Research Center, The University of Texas at El Paso, El Paso, Texas 79968, United States; Imaging & Behavioral Neuroscience (IBN) Facility, College of Science, The University of Texas at El Paso, El Paso, Texas 79968, United States*

Sylvia L. Natividad-Diaz − *Department of Metallurgical, Materials, and Biomedical Engineering, College of Engineering and Border Biomedical Research Center, The University of Texas at El Paso, El Paso, Texas 79968, United States; 3D Microphysiological Systems Laboratory (3DMPSL), The University of Texas at El Paso, El Paso, Texas 79968, United States;* orcid.org/0000-0002-1928-829X

Complete contact information is available at: https://pubs.acs.org/10.1021/acs.nanolett.5c00311

Author Contributions

The manuscript was written through contributions of all authors. All authors have given approval to the final version of the manuscript.

Funding

W.P. acknowledges funding from the University of Texas System STARs Program, the University Research Institute (URI) Award 14648682 from the University of Texas at El Paso, and the University of Texas System Trauma Research and Combat Casualty Care Collaborative (TRC4) award TRC423-ECMR-00061. H.V.B. and A.G. acknowledge the COURI MERITUS UG research fellowships at UTEP from Fall 2023−Spring 2024 for support. J.P. acknowledges support from National Science Foundation (NSF) Grants HRD-408 1826745 and EES-2204750 from the University of Texas System Louis Stokes Alliances for Minority Participation (LSAMP) Program. The authors acknowledge equipment use at the Border Biomedical Research Center, which is generously supported in part by NIH-NIMHD Grant U54MD007592. Additionally, the SmartSPIM light sheet microscope and Imaris workstation are housed in the Imaging & Behavioral Neuroscience (IBN) facility. Research reported in this publication was supported by the Office of The Director, National Institutes of Health (NIH), under award number C06OD032074. The content is solely the responsibility of the authors and does not necessarily represent the official views of the NIH.

Notes

The authors declare the following competing financial interest(s): H.V.B. and W.P. are listed as inventors on a provisional patent application for the research described in this paper. All other authors declare no competing financial interests.

■ ACKNOWLEDGMENTS

The authors would like to acknowledge Dr. Irodiel Vinales and Dr. Katja Michael for technical assistance in reagent quality assessment and processing. Some graphics were, in part, created with BioRender.com.

■ ABBREVIATIONS

LNPs, lipid nanoparticles; SPARKLE, Strategic Peptide Anchored, Retained, and Kept after Lipid Elimination; PET, positron emission tomography; DiI, 1,1′-dioctadecyl-3,3,3′3′-tetramethylindocarbocyanine perchlorate; DiO, 3,3′-dioctadecyloxacarbocyanine perchlorate; DiD, 1,1′-dioctadecyl-3,3,3′,3′-tetramethylindodicarbocyanine, 4-chlorobenzenesulfonate salt; AF647, Alexa Fluor 647; BF568, BP Fluor 568; TNS, 6-(*p*-toluidino)-2-naphthalenesulfonic acid sodium salt; MS, mass spectrometry; HPLC, high-performance liquid chromatography; DBCO, Dibenzocyclooctyne; CLARITY, Clear lipid-exchanged acrylamide-hybridized rigid imaging/immunostaining/in situ-hybridization-compatible tissue hydrogel; WGA, Wheat germ agglutinin; DSPE, 1,2-Distearoyl-sn-glycero-3-phosphoethanolamine; DMG, 1,2-Dimyristoyl-rac-glycerol; PEG, Polyethylene glycol; XTT, 2,3-Bis-(2-methoxy-4-nitro-5-sulfophenyl)-2H-tetrazolium-5-carboxanilide; REMNANT, Retained molecular nanoparticle tag

■ REFERENCES

(1) Nguyen, L. N. M.; Ngo, W.; Lin, Z. P.; et al. The mechanisms of nanoparticle delivery to solid tumours. *Nat. Rev. Bioeng* **2024**, *2*, 201−213.

(2) Yan, L.; Shen, J.; Wang, J.; Yang, X.; Dong, S.; Lu, S. Nanoparticle-Based Drug Delivery System: a Patient-Friendly chemotherapy for oncology. *Dose-Response* **2020**, *18* (3), n/a.

(3) Hsu, J. C.; Nieves, L. M.; Betzer, O.; et al. Nanoparticle contrast agents for X-ray imaging applications. *WIREs Nanomed Nanobiotechnol.* **2020**, *12*, No. e1642.

(4) Shao, K.; Singha, S.; Clemente-Casares, X.; Tsai, S.; Yang, Y.; Santamaria, P. Nanoparticle-Based immunotherapy for cancer. *ACS Nano* **2015**, *9* (1), 16−30.

(5) Cullis, P. R.; Hope, M. J. Lipid nanoparticle systems for enabling gene therapies. *Molecular Therapy* **2017**, *25* (7), 1467−1475.

(6) Banerjee, S. S.; Chen, D. Magnetic Nanoparticles Grafted with Cyclodextrin for Hydrophobic Drug Delivery. *Chem. Mater.* **2007**, *19* (25), 6345−6349.

(7) Chambers, E.; Mitragotri, S. Long Circulating Nanoparticles via Adhesion on Red Blood Cells: Mechanism and Extended Circulation. *Experimental Biology and Medicine.* **2007**, *232* (7), 958−966.

(8) Kamaly, N.; Yameen, B.; Wu, J.; Farokhzad, O. C. Degradable Controlled-Release Polymers and Polymeric nanoparticles: Mechanisms of controlling drug release. *Chem. Rev.* **2016**, *116* (4), 2602−2663.

(9) Dobrovolskaia, M. A.; Aggarwal, P.; Hall, J. B.; McNeil, S. E. Preclinical Studies To Understand Nanoparticle Interaction with the Immune System and Its Potential Effects on Nanoparticle Biodistribution. *Mol. Pharmaceutics* **2008**, *5* (4), 487−495.

(10) Tenchov, R.; Bird, R.; Curtze, A. E.; Zhou, Q. Lipid Nanoparticles−From Liposomes to mRNA Vaccine Delivery, a Landscape of Research Diversity and Advancement. *ACS Nano* **2021**, *15* (11), 16982−17015.

(11) Swetha, K.; Kotla, N. G.; Tunki, L.; Jayaraj, A.; Bhargava, S. K.; Hu, H.; Bonam, S. R.; Kurapati, R. Recent advances in the lipid Nanoparticle-Mediated delivery of mRNA vaccines. *Vaccines* **2023**, *11* (3), 658.

(12) Balcorta, H. V.; Contreras Guerrero, V. G.; Bisht, D.; Poon, W. Nucleic acid Delivery Nanotechnologies for in vivo cell programming. *ACS Applied Bio Materials.* **2024**, *7* (8), 5020−5036.

(13) Anchordoquy, T.; Artzi, N.; Balyasnikova, I. V.; Barenholz, Y.; La-Beck, N. M.; Brenner, J. S.; Chan, W. C. W.; Decuzzi, P.; Exner, A. A.; Gabizon, A.; Godin, B.; Lai, S. K.; Lammers, T.; Mitchell, M. J.; Moghimi, S. M.; Muzykantov, V. R.; Peer, D.; Nguyen, J.; Popovtzer, R.; Simberg, D.; et al. Mechanisms and Barriers in Nanomedicine: progress in the field and future directions. *ACS Nano* **2024**, *18* (22), 13983−13999.
(14) Wilhelm, S.; Tavares, A. J.; Dai, Q.; Ohta, S.; Audet, J.; Dvorak, H. F.; Chan, W. C. W. Analysis of nanoparticle delivery to tumours. *Nature Reviews Materials* **2016**, *1* (5), 1−12.
(15) Poon, W.; Kingston, B. R.; Ouyang, B.; Ngo, W.; Chan, W. C. W. A framework for designing delivery systems. *Nat. Nanotechnol.* **2020**, *15* (10), 819−829.
(16) Uritu, C. M.; Al-Matarneh, C. M.; Bostiog, D. I.; Coroaba, A.; Ghizdovat, V.; Filipiuc, S. I.; Simionescu, N.; Stefanescu, C.; Jalloul, W.; Nastasa, V.; Tamba, B. I.; Maier, S. S.; Pinteala, M. Radiolabeled multi-layered coated gold nanoparticles, as potential biocompatible PET/SPECT tracers. *J. Mater. Chem. B* **2024**, *12* (15), 3659−3675.
(17) Gambhir, S. Molecular imaging of cancer with positron emission tomography. *Nat. Rev. Cancer* **2002**, *2*, 683−693.
(18) Dai, W.; Zhang, J.; Wang, Y.; Jiao, C.; Song, Z.; Ma, Y.; Ding, Y.; Zhang, Z.; He, X. Radiolabeling of Nanomaterials: Advantages and Challenges. *Frontiers in Toxicology* **2021**, *3*, 753316.
(19) Simonsen, J. B.; Kromann, E. B. Pitfalls and opportunities in quantitative fluorescence-based nanomedicine studies−A commentary. *J. Controlled Release* **2021**, *335*, 660−667.
(20) Kamanzi, A.; Zhang, Y.; Gu, Y.; Liu, F.; Berti, R.; Wang, B.; Saadati, F.; Ciufolini, M. A.; Kulkarni, J.; Cullis, P.; Leslie, S. Quantitative visualization of lipid nanoparticle fusion as a function of formulation and process parameters. *ACS Nano* **2024**, *18* (28), 18191−18201.
(21) Im, K.; Mareninov, S.; Diaz, M. F. P.; Yong, W. H. An Introduction to Performing Immunofluorescence Staining. *Methods Mol. Biol.* **2019**, *1897*, 299−311.
(22) Hopwood, D. Fixatives and fixation: a review. *Histochemical Journal* **1969**, *1* (4), 323−360.
(23) Leist, D. P.; Nettleton, G. S.; Feldhoff, R. C. Determination of lipid loss during aqueous and phase partition fixation using formalin and glutaraldehyde. *Journal of histochemistry and cytochemistry: official journal of the Histochemistry Society* **1986**, *34* (4), 437−441.
(24) Kim, J. H.; Jang, M. J.; Choi, J.; et al. Optimizing tissue-clearing conditions based on analysis of the critical factors affecting tissue-clearing procedures. *Sci. Rep* **2018**, *8*, 12815.
(25) Mata Corral, M. Y; Alvarez, D. E; Poon, W. Quantifying nanoparticle delivery: challenges, tools, and advances. *Curr. Opin. Biotechnol.* **2024**, *85*, No. 103042.
(26) Patel, P.; Ibrahim, N. M.; Cheng, K. The Importance of Apparent pKa in the Development of Nanoparticles Encapsulating siRNA and mRNA. *Trends Pharmacol. Sci.* **2021**, *42* (6), 448−460.
(27) Sindhwani, S.; Syed, A. M.; Wilhelm, S.; Glancy, D. R.; Chen, Y. Y.; Dobosz, M.; Chan, W. C. W. Three-Dimensional Optical Mapping of Nanoparticle Distribution in Intact Tissues. *ACS Nano* **2016**, *10* (5), 5468−5478.
(28) Bray, M.; Singh, S.; Han, H.; Davis, C. T.; Borgeson, B.; Hartland, C.; Kost-Alimova, M.; Gustafsdottir, S. M.; Gibson, C. C.; Carpenter, A. E. Cell Painting, a high-content image-based assay for morphological profiling using multiplexed fluorescent dyes. *Nat. Protoc.* **2016**, *11* (9), 1757−1774.
(29) Cimini, B. A.; Chandrasekaran, S. N.; Kost-Alimova, M.; Miller, L.; Goodale, A.; Fritchman, B.; Byrne, P.; Garg, S.; Jamali, N.; Logan, D. J.; Concannon, J. B.; Lardeau, C.; Mouchet, E.; Singh, S.; Shafqat Abbasi, H.; Aspesi, P.; Boyd, J. D.; Gilbert, T.; Gnutt, D.; Carpenter, A. E.; et al. Optimizing the Cell Painting assay for image-based profiling. *Nat. Protoc.* **2023**, *18* (7), 1981−2013.
(30) Guo, Z.; Zheng, Y.; Zhang, Y. CLARITY techniques based tissue clearing: types and differences. *Folia Morphologica* **2022**, *81* (1), 1−12.
(31) Du, H.; Hou, P.; Zhang, W.; Li, Q. Advances in CLARITY-based tissue clearing and imaging. *Experimental and Therapeutic Medicine* **2018**, *16* (3), 1567−1576.
(32) Chung, K.; Wallace, J.; Kim, S.-Y.; Kalyanasundaram, S.; Andalman, A. S.; Davidson, T. J.; Mirzabekov, J. J.; Zalocusky, K. A.; Mattis, J.; Denisin, A. K.; Pak, S.; Bernstein, H.; Ramakrishnan, C.; Grosenick, L.; Gradinaru, V.; Deisseroth, K. Structural and Molecular Interrogation of Intact Biological Systems. *Nature* **2013**, *497* (7449), 332−37.
(33) Syed, A. M.; MacMillan, P.; Ngai, J.; Wilhelm, S.; Sindhwani, S.; Kingston, B. R.; Wu, J. L. Y.; Llano-Suárez, P.; Lin, Z. P.; Ouyang, B.; Kahiel, Z.; Gadde, S.; Chan, W. C. W. Liposome imaging in optically cleared tissues. *Nano Lett.* **2020**, *20* (2), 1362−1369.
(34) Zaleski, M. H.; Chase, L. S.; Hood, E. D.; Wang, Z.; Nong, J.; Espy, C. L.; Zamora, M. E.; Wu, J.; Morrell, L. J.; Muzykantov, V. R.; Myerson, J. W.; Brenner, J. S. Conjugation Chemistry Markedly Impacts Toxicity and Biodistribution of Targeted Nanoparticles, Mediated by Complement Activation. *Adv. Mater.* **2025**, *37* (5), No. e2409945.

https://doi.org/10.1021/acs.nanolett.5c00311
Nano Lett. 2025, 25, 7682−7689